

Synchronous Switch Energy Extraction Circuit for Motor Regenerative Braking Enhancement

Zhiwu Xie¹, Li Teng¹, *Student Member, IEEE*, Yu Yin, and Junrui Liang², *Senior Member, IEEE*

Abstract—The synchronous switch technique has been utilized as a promising solution to enhance the energy harvesting capabilities of piezoelectric devices. It utilizes a switched inductive branch to compensate for the capacitive source and increase the real power. The synchronous switch technique was also extended to enhance energy harvesting from electromagnetic (EM) sources. This brief introduces a synchronous switch energy extraction (SSEE) circuit and examines its performance in motor regenerative braking (RB) enhancement. In the SSEE scheme, a switched capacitive branch is connected to compensate for the inductive source of an electromagnetic motor. The output current from a coil is made in phase with the induced voltage source. The braking power is significantly improved. Therefore, the kinetic energy is extracted much faster to brake the motor quickly, while a portion of the extracted energy is harvested into storable electrical dc energy. This brief comprehensively evaluates the SSEE performances, in terms of energy harvesting and motor braking, respectively. Experimental results show that, given a flywheel released from the same speed, the SSEE can recover 182.5% more energy than the diode-bridge rectifier. For the braking performance, the SSEE can reduce the braking time by 35.1%, compared with the short-circuit braking (SCB) case.

Index Terms—Electromagnetic machine, regenerative braking, ac-dc converter, synchronous switch technique.

I. INTRODUCTION

REGENERATIVE braking (RB) is considered an essential technology for reclaiming the kinetic energy from the moving vehicle and other rotating machines, to realize a more economic and flexible utilization of mechanical drive energy. Compared with the classical mechanical braking method [1], which utilizes the mechanical friction pad to decelerate the

motor and dissipate the regenerated energy in the form of heat, RB not only achieves energy regeneration but also reduces useless heat loss.

So far, researchers have developed many RB methods to improve energy recovery efficiency and braking torque capability. Conventional designs used pulse width modulation (PWM) inverter to realize the RB function [2], [3]. Voltage regulation and braking torque control are implemented within the inverter by applying a proper switching sequence. Due to the limitations of the load voltage and the energy loss in the armature resistance, the PWM-based RB inverter performs less effectively when the motor speed is low [4]. To solve this problem, some researchers used mechanical friction braking to complement the underperformed RB below some low-speed boundaries [5], [6]. The reintroduction of friction braking reduces the energy recovery efficiency. On the other hand, in some studies, a hybrid energy storage module, which adds a supercapacitor to the original battery-powered system, has been utilized to improve the RB performance [7], [8]. The load voltage varies according to the combination structure of the supercapacitor and battery. The influence of the load voltage on the stable performance of the RB process can be reduced. However, the energy transfer between the supercapacitor and battery requires an additional dc-dc converter. In general, a good RB system should be designed by simultaneously improving the *braking capability*, *energy recovery efficiency*, and *load-voltage independence*.

In the research for improving the piezoelectric energy harvesting (PEH) and damping capabilities, there was a promising synchronous switch technique to decouple the piezoelectric source from the load. It is called synchronous electric charge extraction (SECE) [9]. In the piezoelectric source, the internal capacitive component causes a phase lag between the equivalent current source and the voltage across the current source. SECE utilizes a switched inductive branch to compensate for the capacitive source and, therefore, increases the harvested power. Moreover, the switched inductor also serves as an energy transfer medium from the piezoelectric source to the load. The energy of the piezoelectric source is first transferred to the switched inductor and then from the switched inductor to the load. The source-load decoupling design in SECE eliminates the influence of load variation against stable harvested power.

Given the reciprocal relationship between a piezoelectric source (a current source in parallel with a capacitor) and an electromagnetic (EM) source (a voltage source in series with an inductor), the validated synchronous switch technique in

Manuscript received 7 February 2023; revised 2 March 2023; accepted 5 March 2023. Date of publication 9 March 2023; date of current version 12 May 2023. This work was supported in part by the National Natural Science Foundation of China under Grant 62271319 and Grant U21B2002, and in part by the Natural Science Foundation of Shanghai under Grant 21ZR1442300. This brief was recommended by Associate Editor A. Tofighi Zavareh. (Zhiwu Xie and Li Teng are co-first authors.) (Corresponding author: Junrui Liang.)

Zhiwu Xie, Yu Yin, and Junrui Liang are with the School of Information Science and Technology and the Shanghai Engineering Research Center of Energy Efficient and Custom AI IC, ShanghaiTech University, Shanghai 201210, China (e-mail: xiezhw@shanghaitech.edu.cn; yinyu@shanghaitech.edu.cn; liangjr@shanghaitech.edu.cn).

Li Teng is with the School of Information Science and Technology, ShanghaiTech University, Shanghai 201210, China, also with the Shanghai Institute of Microsystem and Information Technology, Chinese Academy of Sciences, Shanghai 200050, China, and also with the University of Chinese Academy of Sciences, Beijing 100049, China (e-mail: tengli@shanghaitech.edu.cn).

Color versions of one or more figures in this article are available at <https://doi.org/10.1109/TCSII.2023.3254807>.

Digital Object Identifier 10.1109/TCSII.2023.3254807

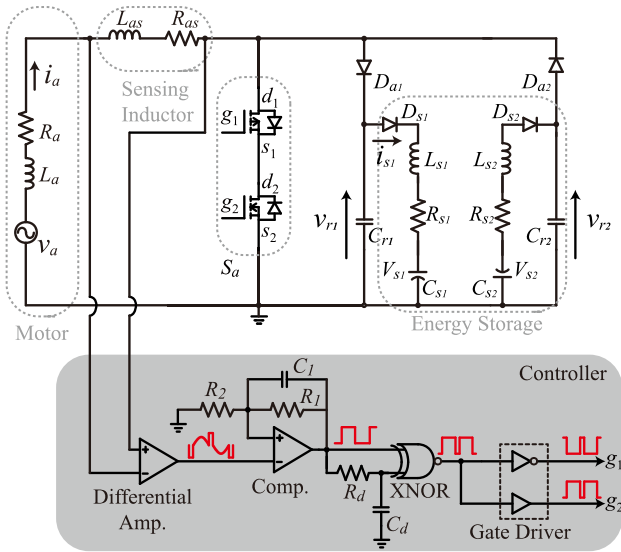


Fig. 1. Topology of the proposed SSEE circuit.

the piezoelectric case was extended to the EM area [10]. Improvements by using a synchronous switch technique are more significant when the effect of the reactive component is more dominant over the resistive component, i.e., when the inductive source impedance has a larger quality factor. Taking the permanent magnet motor as an example, it is a classical EM machine. Usually, its inductive reactance is more significant than the resistance. The motor acts as a generator when operating in the braking state. Thus, the synchronous switch technique is a good candidate for the motor RB. This brief introduces a synchronous switch energy extraction (SSEE) circuit to improve motor RB performance.

II. CIRCUIT PRINCIPLE

The topology of the proposed SSEE circuit is shown in Fig. 1. It can be divided into four parts: the equivalent circuit of a motor, the sensing inductor, the switched capacitive branches, and the energy storage branches. The equivalent circuit of a motor contains the inductance of the coil L_a , the parasitic resistance R_a , and the induced voltage v_a . The switched capacitive branch is formed by a bidirectional switch S_a , which is composed of an N-channel and a P-channel MOSFET, two diodes D_{a1} and D_{a2} , and two resonant capacitors C_{r1} and C_{r2} . The switched branch is used to rapidly transfer the energy stored in the inductor L_a and reset i_a to zero at each synchronous instant, i.e., the zero-crossing point (ZCP) of v_a . It is essential that the synchronous switch actions should be carried out in time. The ZCPs are identified by sampling the voltage with a sensing inductor L_{as} , whose equivalent series resistance (ESR) is denoted as R_{as} . Such a design does not require an additional sensor to sense the position of the rotor. Inductors L_{s1} , L_{s2} , capacitors C_{s1} , C_{s2} , and diodes D_{s1} , D_{s2} form the energy storage branch. The capacitance of C_{s1} and C_{s2} is designed much larger than that of C_{r1} and C_{r2} . The energy storage branch is used to absorb the energy in the resonant capacitor C_{r1} or C_{r2} during the short-circuit period.

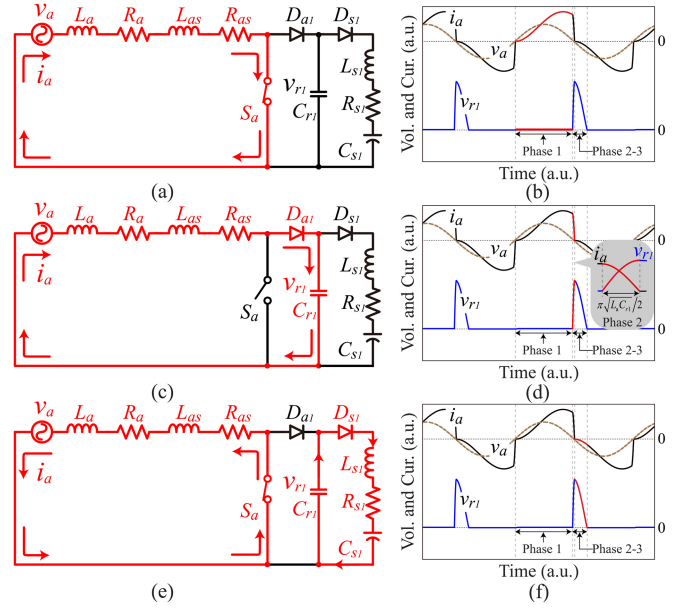


Fig. 2. Circuit and waveform of SSEE in the positive v_a half cycle. (a) and (b) SC phase. (c) and (d) EE phase. (e) and (f) CT phase. (a), (c), and (e) Conducting circuit branches. (b), (d), and (f) Operation waveform.

A. Working Phases

The SSEE circuit can significantly improve the power factor with a low-frequency switch strategy. Each of the positive or negative v_a half cycles can be divided into three phases, the short-circuit (SC) phase, the energy extraction (EE) phase, and the charge transfer (CT) phase. The conducting paths and waveform of the three phases in the positive half cycle of v_a are shown in Fig. 2.

1) *SC Phase*: S_a is closed in almost the positive v_a half cycle, which leaves the EM source in the short-circuit state. The transformed energy is accumulated in the inductor L_a and L_{as} as the integral of the inductor current i_a in this phase.

2) *EE Phase*: Once v_a crosses zero, S_a opens. The energy accumulated in the inductor L_a and L_{as} is rapidly extracted by the resonant capacitor C_{r1} in one-fourth of an LC cycle, i.e., $\pi\sqrt{(L_a + L_{as})C_{r1}/2}$. During this phase, some energy is dissipated in parasitic ESRs R_a and R_{as} , as well as diode D_{a1} . This switch action changes the polarity of i_a by utilizing the transient response of an under-damped RLC branch, which is formed by C_{r1} , L_a , R_a , L_{as} , and R_{as} . Fig. 2(d) shows the operation waveform and the enlarged view of i_a and v_{r1} in this phase.

3) *CT Phase*: When the EE phase is finished, S_a is closed again. The EM source starts the energy accumulation of the negative v_a half cycle. The conducting loop on the left, as shown in Fig. 2(e), is the same as that in the SC phase. The right conducting loop discharges C_{r1} . The extracted energy is now transferred from C_{r1} to the storage capacitor C_{s1} through the energy storage branch, which is formed by C_{r1} , D_{s1} , L_{s1} , R_{s1} , and C_{s1} . Since the voltage source v_a is only involved in the SC and EE phases, the charging process for C_{s1} in this CT phase is independent of v_a . Therefore, like SECE in PEH, SSEE achieves load independence for energy harvesting from an EM source.

B. ZCP Sensing

EE actions must be taken at the ZCP instants of the voltage source v_a . However, v_a is an equivalent element inside the motor. Its ZCP cannot be detected directly. In most motor drive systems, Hall effect sensors provide the classical solution for sensing the position of the rotor and indicating the ZCP of the equivalent voltage v_a . In this brief, we use an external inductor L_{as} to sample the ZCP of v_a during the SC phase. Given the conducting path shown in Fig. 2(a), the frequency-domain representation of the inductor current i_a is formulated as follows

$$I_a(j\omega) = \frac{V_a(j\omega)}{j\omega L_a + R_a + j\omega L_{as} + R_{as} + R_{ds(on)}}, \quad (1)$$

where $R_{ds(on)}$ is the total on-resistance of S_w . The frequency-domain representation of the voltage v_{as} across the inductor L_{as} can be derived as follows

$$V_{as}(j\omega) = (j\omega L_{as} + R_{as})I_a(j\omega). \quad (2)$$

To obtain the ZCP, the inductance L_{as} and resistance R_{as} are designed to be smaller than L_a and $R_a + R_{ds(on)}$, respectively. If we neglect the $j\omega L_{as}$ and R_{as} terms, V_a can be simplified as follows

$$V_a(j\omega) = [j\omega L_a + R_a + R_{ds(on)}]I_a(j\omega). \quad (3)$$

Comparing (2) and (3), the polarity of v_{as} follows that of v_a when the ratio $\omega L_{as}/R_{as}$ is designed to be equal to that of $\omega L_a/[R_a + R_{ds(on)}]$. Thus, the ZCP of v_a can be detected by a sophisticatedly designed sampling inductor L_{as} . Such a sensing method is quite simple and does not rely on an external position sensor.

C. Control Unit

The switch actions are only carried out at the ZCP instants of v_a . An RC delay circuit and some logic gates are utilized to generate such a switch signal. The analog controller is shown in Fig. 1. From the principle of ZCP sampling, v_{as} the voltage across the sensing inductor L_{as} has the same polarity as v_a . The controller uses a differential amplifier to sense the voltage across the inductor L_{as} . In implementations, there is a spike in voltage which is caused by the sudden current change through the sensing inductor during the EE phase. The voltage drop in L_{as} increases the voltage spike. To properly obtain the ZCP and eliminate the influence of the spike voltage in the sampling process, a comparator with an integrator circuit and a hysteresis loop is utilized to carry out this detection task. The comparator converts the ZCP information into the rising or falling edges of a square wave signal. The integrator filters the spike voltage and ensures the square-wave output is stable. After deriving the ZCP information, the turn-off interval of S_a can be controlled by the RC delay circuit and the XNOR gate. One input pin of the XNOR gate is directly connected to the output of the comparator, and the other is connected to the RC delay circuit. Thus, a short output pulse is generated according to the phase shift between the two input signals. The duration of the turn-off interval of switch S_a is about $2R_d C_d$ to $3R_d C_d$. As introduced above, the switch S_a is composed of

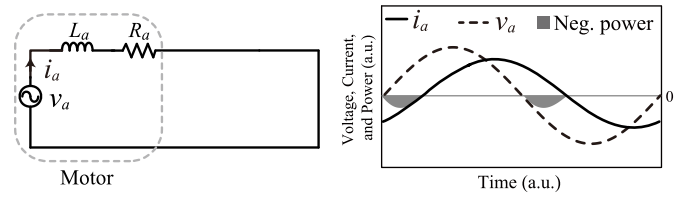


Fig. 3. Circuit and waveform of SCB.

a PMOS g_1 and an NMOS g_2 . Both MOSFETs need to be turned on or turned off simultaneously. Usually, the driving ability of the logic gate is limited. The gate driver is needed to generate complementary signals for g_1 and g_2 with higher driving capabilities.

III. THEORETICAL ANALYSIS

Based on the detailed working principle of the SSEE circuit, this section provides a theoretical analysis of the braking power for evaluating the performance of SSEE in a wide speed range. The braking torque can be formulated as follows

$$T_e = \frac{P_e}{\Omega_s}. \quad (4)$$

where P_e is the braking power; T_e is the braking torque; Ω_s is the motor rotational speed. Formulating the braking power helps evaluate the braking performance.

The short-circuit braking (SCB) method is taken as the benchmark in this brief. The circuit and waveform of SCB are shown in Fig. 3. The induced voltage v_a can be assumed as follows

$$v_a(t) = V_m \sin(\omega t), \quad (5)$$

In the circuit, the motor terminals are directly shorted. The equivalent voltage source only drives the pure internal impedance. Thus, it was regarded as one of the simplest and quickest braking methods [11]. When SCB is applied in the motor braking process, the phase current i_a can be derived as follows

$$i_a(t) = \frac{V_m}{|Z|} \sin(\omega t + \varphi), \quad (6)$$

where $\varphi = \sin^{-1}(\omega L_a/|Z|)$ represents the phase difference between v_a and i_a , $|Z| = \sqrt{R_a^2 + (\omega L_a)^2}$ is the magnitude of the source output impedance. Negative power is found, as shown in Fig. 3(b), given a non-zero φ .

Unlike the passive SCB method, SSEE eliminates the negative power. From the waveform and the conducting path shown in Fig. 2, the current i_a can be formulated with the first-order differential equation

$$v_a(t) = L_1 \frac{di_a(t)}{dt} + R_1 i_a(t), \quad (7)$$

with an initial value

$$i_a(0) = 0, \quad (8)$$

where $R_1 = R_a + R_{as} + R_{ds(on)}$ and $L_1 = L_a + L_{as}$. As the aforementioned ZCP sensing, the inductance L_{as} and resistance R_{as} are designed to be smaller than L_a and $R_a + R_{ds(on)}$,

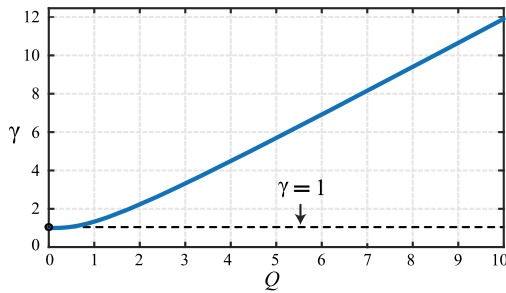


Fig. 4. Braking power comparison ratio between the SSEE and SCB methods.

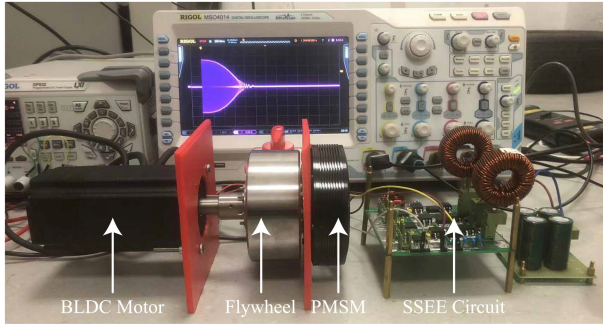


Fig. 5. Experimental setup.

respectively. $R_{ds(on)}$ is usually much smaller than other resistances. Neglecting the L_{as} and $R_a + R_{ds(on)}$ items, (7) can be solved as follows

$$i_a(t) = V_m \frac{e^{-t/\tau} \sin \varphi + \sin(\omega t + \varphi)}{|Z|}, \quad (9)$$

where $\tau = L_a/R_a$ is the time constant of the first-order circuit. The braking power P_e in a cycle is formulated as follows

$$P_e = \frac{1}{T} \int_0^T v_a(t) i_a(t) dt. \quad (10)$$

where T is the duration of each cycle of v_a . By substituting (5), (6), and (9) into (10), the braking power ratio between $P_{e,SSEE}$ in SSEE and $P_{e,SCB}$ in SCB can be derived as follows

$$\gamma = \frac{P_{e,SSEE}}{P_{e,SCB}} = 1 + \frac{2[1 + e^{-\pi/Q}]}{\pi(1 + Q^2)} Q^3, \quad (11)$$

where the quality factor $Q = \omega L_a/R_a$. From the analytical results in Fig. 4, the ratio γ increases significantly with an increasing Q value. The reason is that, in SCB, large Q value enlarges the phase lag between the voltage source v_a and the current i_a . The negative power increases significantly as well, which reduces the performance of SCB. For the SSEE case, it eliminates the negative power regardless of the change in Q value. Therefore, its outperformance over SCB is more significant under large γ .

IV. EXPERIMENT

Experiments are carried out to evaluate the performance of the proposed circuit. The experimental setup is shown in Fig. 5. The parameters of the whole system are listed in Table I. The prototype consists of a permanent magnet synchronous motor (PMSM) and a brushless dc motor (BLDC).

TABLE I
CIRCUIT PARAMETERS

Component	Value / Type
PMSM's inductance L_a , resistance R_a	1 mH, 1.7 Ω
Sensing inductance L_{as} , resistance R_{as}	20 μ H, 25 m Ω
Capacitor $C_{r1,2}$, $C_{s1,2}$	11 μ F, 1000 μ F
Inductance $L_{s1,2}$, Resistance $R_{s1,2}$	1 mH, 50 m Ω
Differential amplifier, comparator	INA126, LMC7211
XNOR gate, Driver	CD4077, UCC27425
Filter elements R_1 , R_2 , C_1	10 M Ω , 30 K Ω , 5 nF
Delay circuit elements R_d , C_d	150 K Ω , 1 nF

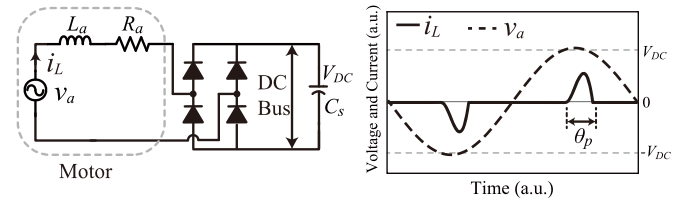


Fig. 6. Circuit and waveform of SEH circuit.

The PMSM is the tested object carrying out the regenerative braking process. The SSEE circuit is connected to the PMSM to harvest the kinetic energy and slow its rotation. The BLDC acts as a driver to provide an initial speed to the PMSM. During the braking process, the power supply to the BLDC is cut off. The PMSM is axially connected to the BLDC with a mechanical coupler. An additional flywheel is mounted on the shaft to increase the kinetic energy at release.

In the braking process, the motor's current and voltage profiles reflect its rotation condition. In the experiment, the initial speed of the braking process is set to 2940 rpm. Fig. 7(a) shows that the motor takes 8 seconds to stop from the initial speed when the circuit is open circuit. When using the SCB method, the braking time can be significantly reduced to 1.48 seconds, as shown in Fig. 7(b). When using SSEE, the braking time can be further reduced to 0.96 seconds, as shown in Fig. 7(c). Fig. 7(f) illustrates the detailed waveform in SSEE. It shows that the switch actions are only carried out twice in one cycle. The inductor current i_a quickly drops to zero after taking the switch actions. From the current waveform of i_a shown in Fig. 7(b), the current drops slowly in the first half of the SCB braking time. The reason for this phenomenon is that the SCB method generates reactive power at high speed. By reducing reactive power throughout the braking process, the SSEE method stops the motor much faster.

The diode-bridge rectifier is regarded as a benchmark to compare the energy harvesting ability, which is named the standard energy harvesting (SEH) circuit. The circuit and waveform are shown in Fig. 6. In the SEH circuit, the energy storage capacitor C_s connects to the full diode bridge. It can simulate the effect of the load voltage V_{DC} on the motor braking process. With the voltage V_{DC} increases, the conduction angle θ_p of the SEH is reduced [12]. When the magnitude of the v_a is lower than the voltage V_{DC} , the braking energy can not return to energy storage capacitor C_s . The energy harvesting ability of SEH is limited. Fig. 7 (d) and (e) show the harvested energy of SEH and SSEE, respectively. From

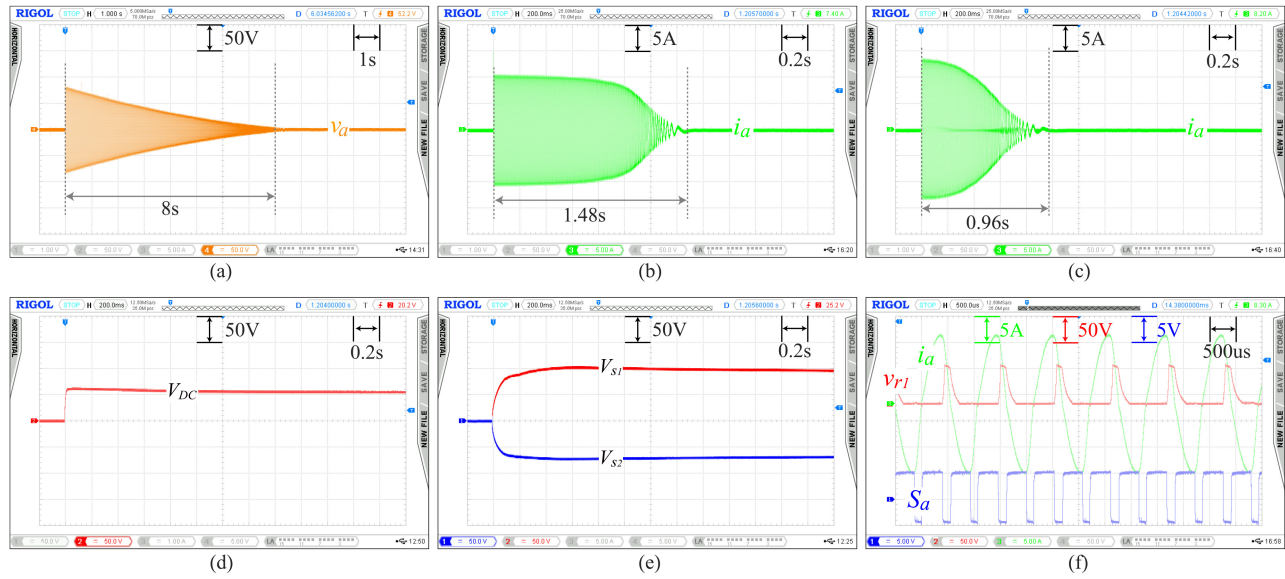


Fig. 7. Experimental waveform. (a) Open-circuit voltage v_a . (b) Output current i_a in SCB. (c) Output current i_a in SSEE. (d) Storage voltage V_{DC} in SEH. (e) Storage voltages V_{s1} and V_{s2} in SSEE. (f) Enlarged waveform in SSEE.

TABLE II
QUALITATIVE COMPARISON OF DIFFERENT RB METHODS

Method	Switch Freq.	Complexity	Advantage	Disadvantage
Classic inverter using PWM control [2], [3]	High	Medium	- Voltage regulation and torque control can be simultaneously realized.	- Source and load are coupled.
Classic inverter with battery/supercapacitor [7], [8]	High	High	- Improve the braking performance in low speed range.	- Source and load are coupled. - An additional dc-dc converter is needed.
Proposed SSEE	Low	Low	- Source and load are decoupled. - It provides a high braking torque.	- The braking torque is unable to be flexibly adjusted at this stage.

the experimental results, the SSEE can harvest 182.5% more energy than the SEH. The harvesting ability is significantly enhanced.

Table II compares the SSEE with several classical RB methods to clearly illustrate the characteristics of the proposed SSEE technique.

V. CONCLUSION

This brief proposed a synchronous switch energy extraction (SSEE) circuit for motor regenerative braking (RB). This circuit can significantly reduce the braking time and enhance the energy harvesting capability of an EM machine. Experiments are carried out to validate the performance of SSEE. The experiment shows that, compared with the standard energy harvesting (SEH) diode-bridge rectifier, SSEE can harvest up to three-fold energy. The braking time is reduced by 35.1% when using the SSEE, compared with the short-circuit braking (SCB) case. The SSEE provides a promising energy extraction mechanism for the electromagnetic inductive machine.

REFERENCES

- [1] K. Zhang, H. Shang, J. Xu, J. Niu, and Y. Yue, "Self-excited, electromagnetic braking and heating system for electric buses," *IEEE Trans. Veh. Technol.*, vol. 71, no. 12, pp. 12543–12551, Dec. 2022.
- [2] B. Saha, B. Singh, and A. Sen, "Solar PV integration to e-rickshaw with regenerative braking and sensorless control," *IEEE Trans. Ind. Appl.*, vol. 58, no. 6, pp. 7680–7691, Nov./Dec. 2022.
- [3] P. Fan, R. Ma, Y. Zhang, Z. Dang, and T. Li, "Bipolar modulation of brushless DC motor with integrated control of motoring and regenerative braking," *J. Power Electron.*, vol. 22, pp. 234–242, Jan. 2022.
- [4] S. Heydari, P. Fajri, M. Rasheduzzaman, and R. Sabzehgar, "Maximizing regenerative braking energy recovery of electric vehicles through dynamic low-speed cutoff point detection," *IEEE Trans. Transp. Electr.*, vol. 5, no. 1, pp. 262–270, Mar. 2019.
- [5] S. Heydari, P. Fajri, R. Sabzehgar, and A. Asrari, "Optimal brake allocation in electric vehicles for maximizing energy harvesting during braking," *IEEE Trans. Energy Convers.*, vol. 35, no. 4, pp. 1806–1814, Dec. 2020.
- [6] X. Zhang, D. Göhlich, and J. Li, "Energy-efficient torque allocation design of traction and regenerative braking for distributed drive electric vehicles," *IEEE Trans. Veh. Technol.*, vol. 67, no. 1, pp. 285–295, Jan. 2018.
- [7] Y. Cao, T. Shi, Y. Yan, X. Li, and C. Xia, "Braking torque control strategy for brushless DC motor with a noninductive hybrid energy storage topology," *IEEE Trans. Power Electron.*, vol. 35, no. 8, pp. 8417–8428, Aug. 2020.
- [8] O. Salari, K. H. Zaad, A. Bakhshai, and P. Jain, "Reconfigurable hybrid energy storage system for an electric vehicle DC-AC inverter," *IEEE Trans. Power Electron.*, vol. 35, no. 12, pp. 12846–12860, Dec. 2020.
- [9] J. Wang, Z. Chen, Z. Li, J. Jiang, J. Liang, and X. Zeng, "Piezoelectric energy harvesters: An overview on design strategies and topologies," *IEEE Trans. Circuits Syst. II, Exp. Briefs*, vol. 69, no. 7, pp. 3057–3063, Jul. 2022.
- [10] E. Arroyo and A. Badel, "Electromagnetic vibration energy harvesting device optimization by synchronous energy extraction," *Sens. Actuat. A, Phys.*, vol. 171, no. 2, pp. 266–273, 2011.
- [11] M. Chandrakanta, A. A. Mahapatra, and A. Sahoo, "Comparative analysis of electrical braking performance for induction motor drive," in *Proc. Technol. Smart-City Energy Security Power (ICSESP)*, 2018, pp. 1–6.
- [12] J. Liang, C. Ge, and Y.-C. Shu, "Impedance modeling of electromagnetic energy harvesting system using full-wave bridge rectifier," in *Proc. Active Passive Smart Struct. Integr. Syst. (SPIE SS/NDE)*, Apr. 2017, Art. no. 101642N.